Colloid and Interface Science Communications 63 (2024) 100811

Contents lists available at ScienceDirect

Colloid and Interface Science Communications

journal homepage: www.elsevier.com/locate/colcom

Rapid Communication

Spongosome-based co-delivery of curcumin and Piperine: A novel strategy for mitigating pollution-induced skin damage

Agnese Bondi [a], Francesca Ferrara [a], Walter Pula [a], Paolo Mariani [b], Alessia Pepe [b], Markus Drechsler [c], Leda Montesi [d], Stefano Manfredini [e], Giuseppe Valacchi [f,g,h,**], Elisabetta Esposito [a,*]

[a] Department of Chemical, Pharmaceutical and Agricultural Sciences, University of Ferrara, I-44121-Ferrara, Italy
[b] Department of Life and Environmental Sciences, Università Politecnica delle Marche, I-60131 Ancona, Italy
[c] Bavarian Polymer Institute (BPI) Keylab "Electron and Optical Microscopy", University of Bayreuth, D-95440 Bayreuth, Germany
[d] Cosmetology Center, University of Ferrara, I-44121 Ferrara, Italy
[e] Department of Neurosciences and Rehabilitation, University of Ferrara, I-44121 Ferrara, Italy
[f] NC State University, Plants for Human Health Institute, Animal Science Dept. NC Research Campus, Kannapolis, NC 28081, USA
[g] Kyung Hee University, Department of Food and Nutrition, Seoul, South Korea
[h] Department of Environmental Science and Prevention, University of Ferrara, I-44121 Ferrara, Italy

ARTICLE INFO

Keywords:
Glyceryl monooleate
Skin
Spongosomes
Curcumin
Piperine
Diesel exhaust emission

ABSTRACT

The present study aims to explore the potential role of curcumin and piperine loaded spongosomes to protect the skin against pollution-induced damage. The hydration of a glyceryl monooleate and sodium cholate thin film, followed by homogenization, led to dispersions with an internal spongiform structure, as demonstrated by cryogenic transmission electron microscopy and small angle X-ray scattering. Spongosome mean diameter measured by photon correlation spectroscopy was roughly 200 nm. Curcumin and piperine were efficiently encapsulated in spongosomes, as demonstrated by ultrafiltration and HPLC analysis. In vitro permeation tests revealed that piperine enhances the penetration of curcumin, suggesting a further improved bioavailability and sustained release. Ex vivo studies using human skin biopsies showed that curcumin and piperine-loaded spongosomes protect the skin against diesel exhaust emissions, preserving the levels of key skin barrier proteins, as filaggrin and involucrin. The formulations exhibited non-irritating properties in human patch tests, supporting their suitability for topical application.

1. Introduction

The skin is the first defence line between the body and the outside world, representing a barrier against external aggression. Nevertheless, prolonged exposure to external insults such as pollutants leads to the formation of reactive oxygen species (ROS) and the generation of bioactive molecules that can affect cellular structure and functions [1]. Endogenous antioxidant defences may not be able to counteract the damaging effects induced by ROS, resulting in cellular impairment and disturbance of skin barrier function. Alterations in *stratum corneum* lipid metabolism as well as the functionality of protein components can promote the development of several skin diseases and disorders [1]. Notably, excessive exposure to UV rays, as well as many air pollutants including smoke exposure, factory emissions, and automobile exhaust can be associated with the development of skin conditions [2,3].

Diesel exhaust emissions (DEE), the most common outdoor pollutants worldwide, comprise a complex mixture of solid, condensed, and gaseous fractions. Both short- and long-term exposure to DEE toxicants is associated with oxidative stress and inflammation, which can accelerate the skin aging process, or the onset of diseases such as atopic dermatitis, acne, psoriasis, androgenetic alopecia, and skin cancers [4]. In this respect, the administration of molecules able to prevent the skin

Abbreviations: GMO, Glyceryl monooleate; SP, Spongosomes; CR, Curcumin; PP, Piperine; DEE, Diesel exhaust emission.

* Corresponding author.
** Corresponding author at: NC State University, Plants for Human Health Institute, Animal Science Dept. NC Research Campus, Kannapolis, NC 28081, USA.
E-mail addresses: agnese.bondi@unife.it (A. Bondi), frrfnc3@unife.it (F. Ferrara), walter.pula@unife.it (W. Pula), leda.montesi@unife.it (L. Montesi), mascia.benedusi@unife.it (S. Manfredini), vlcgpp@unife.it (G. Valacchi), ese@unife.it (E. Esposito).

https://doi.org/10.1016/j.colcom.2024.100811
Received 4 September 2024; Received in revised form 18 November 2024; Accepted 20 November 2024
Available online 29 November 2024

oxidative insult can restore the homeostasis skin defence mechanism [5,6]. Particularly phytocompounds such as curcumin (CR) and piperine (PP) (Fig. S1) possessing antioxidant and anti-inflammatory properties, could offer a "green" alternative to synthetic molecules.

CR is the active component of turmeric (*Curcuma longa*), commonly used as a spice ingredient and known for its wide range of therapeutic properties, including anti-inflammatory, antioxidant, antimicrobial, anti-neoplastic, antiviral, and anti-arthritic effects [7,8]. CR may be effective in the treatment of several skin conditions such as atopic and iatrogenic dermatitis, wound care, acne, pruritus, psoriasis, skin aging, cancer, and infections [9]. Nonetheless, CR possesses low solubility and poor bioavailability, requiring a specialized delivery system capable of maintaining and promoting its activity [10]. PP is an alkaloid principally isolated from *Piper nigrum*, possessing anticancer, antioxidant, antidiabetic, anti-obesity, cardioprotective, antimicrobial, antiaging, immunomodulatory, hepatoprotective, anti-allergic, anti-inflammatory, and neuroprotective properties [11]. Moreover, PP can enhance the oral bioavailability of co-administered drugs and nutrients through several different pathways [12]. Namely, some studies have demonstrated the efficacy of PP in increasing CR topical absorption, suggesting a penetration enhancer role [13].

In this respect, recently we demonstrated the potential of CR and PP, separately loaded into phosphatidylcholine based vesicular systems, in preventing environmental-stressor-induced skin damage [14]. Thus, in the present study, we further explored the possibility of administering both molecules on the skin using a single lipid supramolecular system based on glyceryl monooleate (GMO).

GMO is a biodegradable and non-toxic unsaturated monoglyceride able to self-assemble in water into different liquid crystalline structures, including lamellar, cubic, hexagonal, and sponge phases [15]. GMO dispersion in water, in the presence of surfactants, under a high energy input and specific temperature, leads to lipid nanostructures with inner lyotropic liquid crystalline phase. These lipid supramolecular systems represent attractive nanoplatforms for drug delivery, due to their biocompatibility and biodegradability, efficacy to entrap both hydrophilic and hydrophobic molecules, capability to control drug release, high versatility (stimuli-responsive behaviour) and cost-effective manufacture [16]. Moreover, the structural similarity of GMO dispersions with *stratum corneum* lipid structure makes them particularly suitable for skin administration of active ingredients [17,18].

The type of surfactants and preparation modalities influence the formation of different lipid nanostructures, such as cubosomes, hexasomes, or spongosomes (SP). The latter are characterized by an inner "sponge" mesophase organization, a bicontinuous phase less ordered and more fluid compared to cubic phases and classified as "L3" [15,19,20]. The SP architecture presents open structures consisting of a highly convoluted and interconnected three-dimensional network, in which bicontinuous lipid bilayers intersect with nanometer-sized aqueous channels, allowing to entrap either hydrophilic or hydrophobic molecules [19].

With respect to liposomes, cubosomes and spongosomes possess a nanochannel network organization enabling a higher drug encapsulation efficacy and sustained release. In addition, cubosome and spongosome advantages with respect to liposomes are related to their larger specific surface area and longer stability, enabling to storage them for long time without phase separation or particle size increase [15–17].

CR can be efficiently co-loaded in SP, for instance, Rakotoarisoa et al. investigated the neuroprotective potential of these nanostructures as delivery systems of CR in association with fish oil. Indeed, the SP large lipid/water interface area enables to solubilize both hydrophilic and lipophilic drugs [19].

In the present study, the possibility of co-loading PP and CR in SP was investigated to obtain a single lipid-based dispersion suitable for topical administration. Particularly, the formulation should improve CR oxinflammatory power [21] and protect the skin against environmental-induced skin damage.

2. Materials and methods

2.1. Materials

Curcumin (1*E*,6*E*)-1,7-bis(4-hydroxy-3-methoxyphenyl)hepta-1,6-diene-3,5-dione, purity grade 94 %, CR) and piperine ((2*E*,4*E*)-5-(1,3-benzodioxol-5-yl)-1-piperidin-1-ylpenta-2,4-dien-1-one, purity grade 97 %, PP) were purchased from *Merck Life Science S.r.l.* (Milan, Italy). Glyceryl monooleate (GMO) was purchased from *Ataman Chemicals* (Instanbul, Turkey); sodium cholate hydrate (NaChol) and casein sodium salt from bovine milk (NaCas) were provided by Sigma-Aldrich (St. Louis, Missouri, USA). Nylon membranes and STRAT-M® membranes were purchased from *Merck Life Science S.r.l.* (Milan, Italy). Solvents were HPLC grade, and all other chemicals were analytical grade.

2.2. Preparation of glycerol monooleate aqueous dispersion

GMO dispersions were prepared by thin-film hydration and homogenization. The first step consisted of the solubilization of GMO and NaChol in ethanol at room temperature. Subsequently, the ethanol was evaporated using a rotavapor (Heidolf vv2000, Schwabach, Germany) at 60 °C, leading to the formation of a thin lipid film. The film was hydrated with water (pre-heated at the same temperature) or Na-Cas water solution, and then vortexed for 5 min. The second step consisted of homogenization of the preheated dispersion (60 °C) using ULTRA-TURRAX T 10 basic (IKA WERKE) at 25000 rpm for 1 min. Afterwards, the formulation was cooled to 22 °C and water was added to restore any lost volume to a final volume of 5 mL. In case of drug loaded formulations, CR and PP, separately (0.25, 0.5 mg/mL) or combined (CR 0.25-PP 0.25, or CR 0.4-PP 0.1 mg/mL) were previously solubilized in ethanol used in the very first production step.

2.3. Cryo transmission Electron microscopy (Cryo-TEM)

Cryo-TEM was selected to evaluate the structure of GMO dispersions. This technique requires sample vitrification as previously reported [22]. The method is reported in Supplementary materials (S.1.1).

2.4. X-ray scattering analysis

Small-angle X-ray scattering (SAXS) experiments were performed at SAXS beamline at the Elettra Synchrotron in Trieste (Italy). The method is reported in Supplementary materials (S.1.2).

2.5. Photon correlation spectroscopy (PCS)

Size distribution was evaluated using Zetasizer Nano-S90 (Malvern Instr., Malvern, England), as reported in Supplementary materials (S.1.3). *Z*-Average and polydispersity index values of GMO dispersions were measured. Particularly, 6 different independent batches for each type of dispersions were evaluated, calculating mean values and standard deviations.

2.6. Entrapment capacity

To quantify the entrapment of the drugs within the SP, ultrafiltration (Microcon centrifugal filter unit with YM-10 membrane, NMWCO 10 kDa, Sigma-Aldrich, St. Louis, MO, USA), followed by a high-performance liquid chromatography (HPLC) analysis method was employed, as reported in Supplementary materials (S.1.4). The entrapment capacity (EC) was calculated as follows:

$$EC = D/T_D \times 100 \quad (1)$$

In the equation, D parameter refers to the amount of drug associated with the SP and T_D represents the real drug content in the entire formulation.

2.7. Franz cells methodology

Franz diffusion cells (PermeGear Inc., Hellertown, PA, USA) were employed for in vitro permeation test (IVPT). The apparatus consists in two chambers (donor and receptor compartment) separated by a membrane with a surface area of 0.78 cm^2. In order to reproduce sink conditions, the receptor compartment was filled with 5 mL of ethanol: water mixture (50:50, *v*/v), stirred magnetically at 500 rpm, while kept at 32 ± 1 °C. The methodology is reported in Supplementary materials (S.1.5).

2.8. In vitro permeation tests (IVPTs)

For the IVPT data analysis, the amount of CR and PP (μg/cm^2) permeated through the membrane was plotted over time. Several parameters are needed to characterize the permeation process.

Firstly, 'Jss', which represents the steady-state flux, is given by the equation:

$$Jss = P \times Cd \times D/e \quad (2)$$

'P' is the partition coefficient, 'Cd' is the drug concentration in the donor compartment, 'D' is the drug diffusion coefficient and 'e' is the membrane thickness, provided by the manufacturer.

From those parameters it is possible to calculate the permeability coefficient, 'Kp', and the lag time, 'Tlag' as follows:

$$Tlag = e^2/6 \times D \quad (3)$$

$$Kp = D \times P/e \quad (4)$$

In addition, the permeated amount of drug was expressed as a percentage of the amount of drug loaded in the formulations.

2.9. HPLC analysis

The HPLC analyses were carried out using Perkin Elmer Series 200 HPLC Systems (PerkinElmer, Waltham, MA, USA), equipped with a micropump, an autosampler, and an UV detector, in isocratic conditions. Specifically, stainless steel C-18 reverse-phase column (15 × 0.46 cm) packed with 5 μm particles (Hypersil BDSC18 Thermo Fisher Scientific S.p.A., Milan, Italy) was eluted with a mobile phase composed by methanol/water 80:20 *v*/v using a flow rate of 1 mL/min. The injection volume was 5 μL, and the retention times were 2.3 min and 2.7 min for CR and PP respectively. Wavelength was set to 360 nm for CR and 243 nm and for PP. In case of samples containing both drugs the wavelength was set to 360 nm.

2.10. Stability study

The effect of storage on dispersions was investigated on samples kept at 4 °C for 2 months. Size stability was evaluated repeating PCS analyses after 60 days as previously reported.

2.11. Patch test

A study on human volunteers was conducted to assess the skin irritation potential of SP formulations loaded with CR and PP following a single application to the skin, observing standardized protocols for evaluating the skin compatibility of cosmetic ingredients [23]. The methodology is reported in Supplementary materials (S.1.6).

2.12. Biological activity studies

2.12.1. Human specimens

Human skin explants were obtained from elective abdominoplasties from 3 different donors (caucasian females) after the approval of the Institutional Biosafety (IBC) Committee at NC State University. As previously reported [14,24], skin biopsies were cut with a 12 mm diameter punch and deprived of the subcutaneous fat tissue. Afterward, the skin biopsies were briefly washed in Phosphate Buffer Solution (PBS) and put into 6-well plates filled with 1 mL of DMEM High Glucose medium supplemented with 10 % Fetal Bovine Serum (FBS), 100 IU/mL penicillin and 100 mg/mL streptomycin. The plates were incubated at 37 °C in a 5 % CO2/95 % air atmosphere for one night before the treatment.

2.12.2. Treatment and exposure to DEE

After overnight recovery, the skin biopsy medium was replaced with 1 mL of fresh complete medium, the samples were treated or not with the indicated formulations and exposed to DEE as previously described [25]. The methodology is reported in Supplementary materials (S.1.7).

2.12.3. Collection of tissues and Immunohistochemical analysis

After the second exposure the skin explants were collected and fixed in 10 % neutral buffered formalin for 48 h at 4 °C then dehydrated and embedded in paraffin. The methodology performed as previously described [3] is reported in Supplementary materials (S.1.8).

2.13. Statistical analysis

Statistical analysis was performed using GraphPad Prism 9 (Version 9.4.1 (458), GraphPad Software Inc., La Jolla, CA, USA). For each of the variables tested, an analysis of variance (1-way or 2-way ANOVA), followed by Tukey's post hoc test, was assessed. Each data is the mean ± SD of triplicate determinations obtained in three independent experiments. The p value <0.05 was considered statistically significant. For all the experiments, the control values were set to 1.0, and the other values were expressed as a fold change.

3. Results and discussion

3.1. Preparation and characterization of GMO dispersions

The purpose of this study is to develop GMO-based liquid crystalline structures for the transdermal delivery of CR and PP, in combination. Many studies in the food field have demonstrated the advantages of simultaneously administering phytocompounds such as CR, PP, quercetin, genistein, and coenzyme Q10 to improve their bioaccessibility and control their chemical degradation [26].

In the first part of the work, a pre-formulatory study was performed to obtain GMO dispersions suitable for CR and PP solubilization. Table 1 reports the composition of GMO dispersions stabilized by NaChol (GD1), or by a mixture of NaChol and NaCas (GD2). Dispersions appeared milky, homogeneous, and free from aggregation.

In a previous study [27] GMO dispersions were prepared by a method based on the emulsification of molten GMO in water in the presence of NaChol and/or NaCas, followed by homogenization. The technological instruments required for the former method led to produce at least 50 mL of dispersions, with a considerable waste of excipients and drugs Conversely, the procedure based on hydration of a thin GMO film obtained by rotary evaporation, followed by homogenization, allowed to 10-fold reduce the volume of GMO dispersions [27]. Moreover, no previously reported aggregation phenomena were observed, confirming the importance of the applied method in the preparation of lyotropic liquid crystalline nanodispersions.

GMO dispersion size distribution parameters, obtained by PCS analysis, are shown in Table 1. Mean diameters, expressed as *Z*-Average, are around 200 nm, slightly larger in the case of GD2, enriched with NaCas in its composition. Polydispersity indexes were around 0.2, indicating homogeneous size distribution.

The addition of the drugs didn't affect GD1 and GD2 appearance, except in the case of CR, resulting in the typical yellow colour.

To shed light on the morphology and the inner supramolecular

Table 1
Composition of GMO dispersions expressed as % *w*/w.

Formulation	GMO[1] % *w/w*	NaChol[2]% *w/w*	NaCas[3]% *w/w*	H_2O %*w/w*	Z Average (nm) ± s.d.	PI[4] ± s.d.
GD1	4.50	0.15	–	95.350	198.38 ± 23.67	0.199 ± 0.04
GD2	4.50	0.15	0.07	95.325	214.65 ± 11.10	0.209 ± 0.01

[1] Glyceryl monoolein; [2] Na cholate; [3] Na caseinate; [4]Polydispersity index.

structure of GMO dispersions, Cryo-TEM and SAXS were employed. Fig. 1 shows spheroidal structures with the typical irregular inner organization of sponge phase, both in the case of GD1 (A) and GD2 (B) [15].

Fig. S2 reports the SAXS spectra of GD1 (A) and GD2 (B) measured at 25 and 37 °C to mimic the temperature conditions of storage and cutaneous application.

For all samples, the SAXS profiles are characterized by a broad correlation peak, centred at $Q_c \approx 1.6$ nm^{-1}, and by a low-intensity narrow peak, centred at $Q_p \approx 1.42$ nm^{-1}. From a qualitative point of view and based on results on dispersed GMO systems [28–30], the observed profiles indicate that two coexisting stable lyotropic liquid-crystalline phases occur simultaneously within the GMO dispersions: a sponge L3 phase, indicated by the broad band, and a hexagonal phase, suggested by the presence and position of the narrow peak. The two-phase system is very stable: the SAXS profiles do not change with temperature and composition, indicating that the two phases are in equilibrium with each other [31].

The structural properties of the sponge phase can be derived considering that GMO in water forms at least 3 different inverted, long-range ordered bicontinuous cubic phases [29], whose structure is described in terms of Infinite Periodic Minimal Surfaces, e.g., infinite arrays of connected saddle surfaces (where lipid monolayers are draped) with zero mean curvature at every point on that surface [32]. In some cases, such as after the addition of NaChol [30], the formation of a "molten cubic phase" (the sponge L3-type phase), always characterized by multiconnected saddle-shaped membranes but without long-range order, has been reported. According to the absence of long-range order, the SAXS profile of the sponge L3 phase shows only one broad peak, just as observed in the present case (Fig. S2). This broad peak is related to the cell-cell bilayer correlations: structural parameters can be then obtained by fitting this peak with Eq. (5),

$$I(Q) = c \Big/ \left(\xi^{-2} + (Q - Q_c)^2\right) \quad (5)$$

where c is a normalization constant, ξ is the correlation length and $L = 2\pi/Q_c$ is a characteristic lipid bilayer correlation distance [28]. Results obtained in the present case are reported in Table 2.

The SAXS profile in Fig. S2 also shows the presence of a narrow peak, superposed to the broad band. To assign this peak, two aspects were taken into consideration: *first*, the value of the hexagonal lattice parameter a, calculated by the peak position Q_p using $a = 4\pi / (Q_p \sqrt{3})$ (see Table 2, footnote 1), matches well the ones observed for the hexagonal phase occurring in monoolein systems [28,29,33]. Second, an inverted hexagonal phase was reported to form in the phase diagram of a similar monoolein mixture between the cubic and the sponge phase at room temperature and in excess of aqueous medium [28]. Therefore, the presence of an inverted hexagonal phase, which co-exists in equilibrium with the sponge phase within the analysed GMO dispersions, was suggested. It should be noticed that the peak corresponding to the hexagonal phase is narrow but of low intensity, so that a very minimal structuring of the dispersed GMO system should occur in this regard, and considering the pre-eminence of the sponge phase, the nanostructures constituting the spheroidal particles observed in the GMO dispersion can be defined as "spongosomes" [28].

As already underlined, Fig. S2 shows that temperature did not affect the SAXS profiles, indicating the same phase co-existence at 25 and 37 °C. Namely, structural parameters change by a small value: on heating, the hexagonal unit cell reduces as well as slightly reduce the bilayers correlation distance in the sponge phase, indicating a shrinking of the bilayer because a higher fluidity of the hydrocarbon chains. By contrast, an increase of the correlation length ξ is observed at 37 °C,

Table 2
Structural parameters for the hexagonal and the sponge L3 phases.[1]

	25 °C			37 °C		
Formulation	a^1 (nm)	L^2 (nm)	ξ^3(nm)	a^1 (nm)	L^2 (nm)	ξ^3 (nm)
GD1	5.11	3.94	2.34	5.09	3.87	2.47
GD2	5.00	3.82	2.35	4.99	3.75	2.49
SP $CR_{0.25}$	5.13	3.97	2.30	5.09	3.89	2.49
SP $PP_{0.25}$	5.13	3.99	2.33	5.09	3.90	2.48

[1] Inverted hexagonal lattice parameter; [2] L3 bilayer correlation distance; [3]Correlation length. Errors are around 2%.

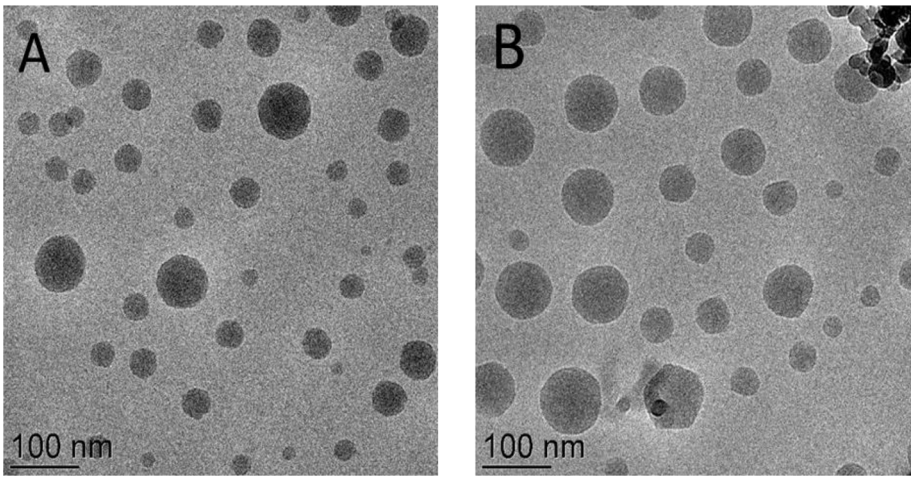

Fig. 1. Cryo-TEM micrographs of GD1 (A) and GD2 (B) formulations.

suggesting increased thermal fluctuations inside the sponge L3 phase.

Notably, X-ray and cryo-TEM analyses demonstrated that the preparation procedure influences the supramolecular organization of the GMO dispersion. Indeed, the previous method led to unilamellar nanovesicles, cubosomes and hexasomes [34], while the new one resulted in nanodispersions with internal sponge phase organization in both GD1 and GD2.

3.2. Preparation of drug loaded spongosomes

Since the preliminary formulative study showed similar size distribution, morphology, and inner structure for GD1 and GD2, to simplify as much as possible the vehicle composition in view of drug loading, GD1 was selected, being based on GMO associated with the single surfactant NaChol. As first approach, CR and PP were separately loaded by previous solubilization in ethanol (0.25 or 0.5 mg/mL), resulting in SP dispersions, as reported in Table 3. The presence of the drugs led to a slight increase (25–35 nm) in the *Z*-Average mean diameters with respect to the empty GD1 (Table 1). PI values slightly increased in the case of the 0.5 mg/mL drug concentration.

SAXS analyses performed on SP $CR_{0.25}$ and SP $PP_{0.25}$ (Fig. 2), confirmed the band and the peak typical of unilamellar vesicles and sponge phase L3, found in the case of the empty GD1 dispersion. According to previous results, the key parameters suggest that the presence of the drugs (CR and PP) does not alter the characteristics of the dispersed system, notably, the characteristic distance *L* related to the correlations between the lipid bilayers in the sponge is quite constant. The value is around 3.95 nm, larger than the GMO bilayer thickness, which is around 3.2 nm; suggesting that the hydration level of GMO in the L3 phase remains low, even when the composition of the dispersion is changed (presence of one or two surfactants, presence of the drugs).

As second approach, both CR and PP were simultaneously loaded into SP dispersions, following two different associations, namely 1:1 and 1:4 CR-PP *w*/w ratios. Composition of the formulations, as well as size distribution parameters obtained by PCS analysis are summarized in Table 3. *Z*-Average mean diameters underwent a slight increase (20 nm) in the case of SP $CR_{0.4}/PP_{0.1}$, while PI was still below 0.25.

3.3. Entrapment capacity evaluation

EC values in SP, obtained by ultrafiltration and HPLC, are summarized in Table S1. It is noteworthy that the production procedure enabled to simultaneously load both CR and PP in SP $CR_{0.4}/PP_{0.1}$ and SP $CR_{0.4}/PP_{0.1}$, with values ranging between 71 and 83 %, both for CR and PP. Indeed, the composition and the peculiar open structure of SP, consisting of a convoluted and interconnected three-dimensional network, confer a high capability to encapsulate lipophilic molecules [15].

3.4. IVPT

IVPT was employed to predict the in vivo permeation of CR and PIP separately or jointly loaded in SP $CR_{0.5}$, SP $PP_{0.5}$, SP $CR_{0.25}/PP_{0.25}$, and SP $CR_{0.4}/PP_{0.1}$. STRAT-M® membrane was selected as a suitable model to mimic *stratum corneum* characteristics. Drug diffusion profiles are shown in Fig. 2, while Table 4 summarizes the calculated diffusion parameters. Drug permeation process consists in two main steps. The first one is described by P, reflecting the preferred distribution of the drug in the skin/membrane or the vehicle. The second step is described by D and Kp coefficients, referring to the diffusion of the drug through the skin (or membrane) depending on its characteristics and vehicle properties.

Fig. 2 clearly shows that in any case PP diffused much faster respect to CR. A lag time (T_{lag}) was detected in all the diffusion kinetics, longer for CR with respect to PP, suggesting that CR was more strongly retained into the SP ultrastructure, due to the major lipophilic character of the drug (logP 3.29) with respect to PP (logP 2.78).

On one hand, in the case of SP $CR_{0.5}$, CR was undetectable in the receptor compartment until 8 h, hampering a detailed evaluation of IVPT parameters, on the other, in SP $CR_{0.25}/PP_{0.25}$ and SP $CR_{0.4}/PP_{0.1}$, where CR was combined with PP, a slow CR diffusion was observed. This phenomenon suggests a possible competition between CR and PP within the ultrastructure, which favoured the expulsion of CR in the presence of PIP.

Notably, Kp values of PP were roughly 4-fold higher with respect to CR, both in the case of SP $CR_{0.25}/PP_{0.25}$ and SP $CR_{0.4}/PP_{0.1}$. Surprisingly, Kp value for CR was 1.6-fold minor in the case of SP $CR_{0.4}/PP_{0.1}$ with respect to SP $CR_{0.25}/PP_{0.25}$, suggesting that the higher the amount of CR, the stronger its retention in the donor phase. The faster permeation of PP with respect to CR in all tested formulations indicates a stronger hydrophobic interaction between CR and the lipophilic supramolecular structure of the spongiform dispersed phase, whose 3D network architecture involves interconnected internal compartments. Moreover, D values of PP were 3-fold higher with respect to CR, both in the case of SP $CR_{0.25}/PP_{0.25}$ and SP $CR_{0.4}/PP_{0.1}$, indicating that PP was more promptly available for diffusion and partition to the membrane with respect to CR. Comparing the co-loaded formulations with SP $PP_{0.5}$, in the case of PP, higher P and Kp values were observed, whilst the D values of PP in the case of SP $CR_{0.25}/PP_{0.25}$ and SP $CR_{0.4}/PP_{0.1}$ were roughly double with respect to SP $PP_{0.5}$, suggesting that the association of CR and PP can promote the diffusion of both drugs. After 24 h, as expected, the amount of diffused PP was much higher with respect to CR, in all tested formulations, while the highest value was obtained for SP $PP_{0.5}$ formulation, containing a higher drug amount. Furthermore, the combination of these two phytocompounds was effective in promoting both PP and CR diffusion across the STRAT-M membrane. The faster diffusion rate found in the case of CR loaded in both SP $CR_{0.25}/PP_{0.25}$and SP $CR_{0.4}/PP_{0.1}$ with respect to SP $CR_{0.5}$, suggests a possible competitive mechanism between the two compound jointly loaded within the SP ultrastructure. The joint presence of CR and PP in SP $CR_{0.25}/PP_{0.25}$ and SP $CR_{0.4}/PP_{0.1}$ could affect the hydrophobic interaction between the drugs and the matrix, with respect to the individually CR-loaded SP $CR_{0.5}$, finally improving CR diffusion [26].

3.5. Patch test

To evaluate the safety of the loaded and unloaded SP applied to the

Table 3
Composition and size distribution parameters of SP loaded with CR and/or PP.

Formulation	GMO[1] %w/w	NaChol[2]%w/w	H_2O %w/w	PP[3]%w/w	CR[4]%w/w	Z-Average (nm) ± s.d.	PI[5] ± s.d.
SP $CR_{0.25}$	4.50	0.15	95.325	–	0.025	223.7 ± 14.4	0.164 ± 0.030
SP $PP_{0.25}$	4.50	0.15	95.325	0.025	–	228.4 ± 13.6	0.178 ± 0.050
SP $CR_{0.5}$	4.50	0.15	95.255	–	0.050	241.1 ± 34.5	0.241 ± 0.021
SP $PP_{0.5}$	4.50	0.15	95.255	0.050	–	232.2 ± 7.6	0.264 ± 0.047
SP $CR_{0.25}/PP_{0.25}$	4.50	0.15	95.255	0.025	0.025	243.0 ± 27.2	0.237 ± 0.048
SP $CR_{0.4}/PP_{0.1}$	4.50	0.15	95.255	0.040	0.010	264.0 ± 62.2	0.233 ± 0.045

[1] Glyceryl monoolein; [2] Na cholate; [3] Piperine; [4] Curcumin; [5]Polydispersity index. Size distribution parameters refer to the mean values of PCS measurements conducted on 6 different independent batches for each type of SP.

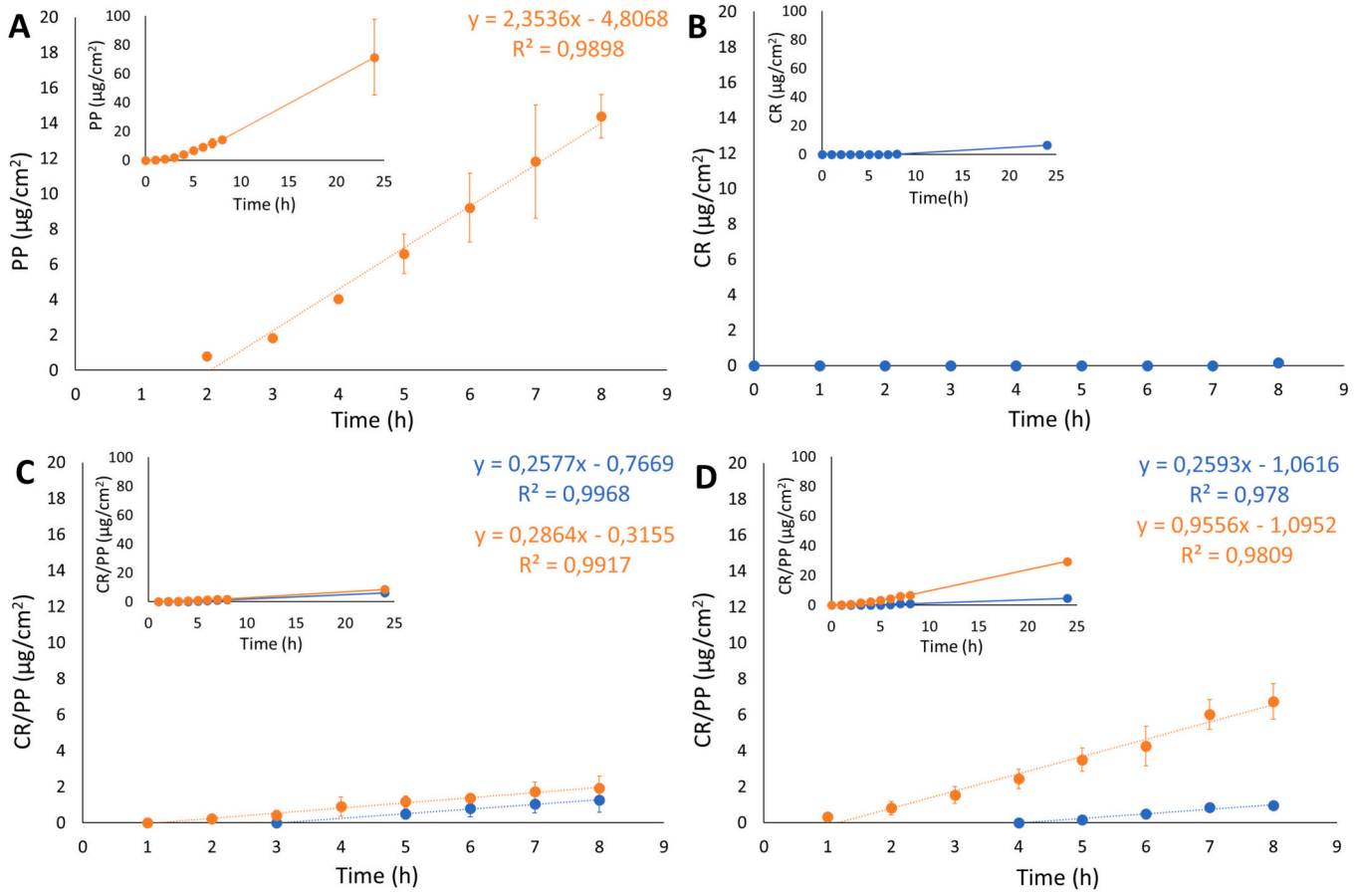

Fig. 2. CR (blu circles) and PP (orange circles) diffusion profiles from SP $CR_{0.5}$ (A), SP $PP_{0.5}$ (B), SP $CR_{0.4}/PP_{0.1}$ (C), and SP $CR_{0.25}/PP_{0.25}$ (D), as determined by Franz cells associated with the STRAT-M® membrane. The insets in each panel refer to the respective 0–24 h kinetics. Data are the mean of 3 independent experiments ± s.d.

Table 4
IVPT parameters of indicated formulations calculated for CUR and PIP respectively.

IVPT Parameters	SP $CR_{0.5}$	SP $PP_{0.5}$	SP $CR_{0.25}/PP_{0.25}$		SP $CR_{0.4}/PP_{0.1}$	
			CR	PP	CR	PP
Jss[1] (µg/cm^2/h)	–	2.35 ± 0.73	0.26 ± 0.01	0.96 ± 0.12	0.26 ± 0.02	0.29 ± 0.12
Kp[2] (cm/h) × 10^3	–	4.71 ± 1.46	1.04 ± 0.02	3.82 ± 0.25	0.64 ± 0.08	2.86 ± 0.92
Tlag[3] (h)	–	2.04 ± 0.04	4.09 ± 0.21	1.15 ± 0.15	2.98 ± 0.16	1.10 ± 1.18
D[4] (cm^2 h^{-1}) × 10^5	–	8.20 ± 1.03	4.09 ± 1.51	14.61 ± 2.52	5.63 ± 0.13	15.20 ± 3.22
P[5]	–	1.82 ± 0.02	0.80 ± 0.01	0.83 ± 0.05	0.36 ± 0.02	0.60 ± 0.02
A[6] (µg/cm^{-2})	6.35 ± 0.03	71.38 ± 26.22	4.65 ± 0.71	29.45 ± 0.31	6.15 ± 1.08	8.60 ± 1.71

[1] Steady-state flux per unit area; [2]permeability coefficient; [3]lag-time; [4]diffusion coefficient; [5]partition coefficient (membrane/vehicle); [6]cumulative amount of drug diffused at 24 h; data are the mean of 3 independent Franz cell experiments ± s.d.

skin, a patch test was conducted on 20 healthy volunteers. Specifically, formulations GD_1, SP $CR_{0.5}$, SP $PP_{0.5}$, and SP $CR_{0.4}/PP_{0.1}$ were tested to evaluate the number of irritative reactions 15 min and 24 h after the removal of the Finn Chamber. Since the reaction was negligible in all cases, the formulations could be classified as non-irritating to the human skin.

3.6. *Ex vivo tests*

Human skin biopsies were used to evaluate the possible protective effect exerted by selected formulations against damage caused by DEE exposure, one of the most aggressive pollutants. Specifically, skin biopsies were pre-treated with SP $CR_{0.5}$, SP $PP_{0.5}$, SP $CR_{0.25}/P_{0.25}$ and SP $CR_{0.4}/PP_{0.1}$ and exposed to DEE; CTRL biopsies remained untreated and unexposed while DEE biopsies were exposed to the pollutant without treatment. Immunofluorescence analyses were carried out on skin tissue to evaluate the expression of key protein involved in the processes of differentiation of the epidermis (involucrin) [35], in the formation of the skin barrier (filaggrin) [36], and in conferring support to the skin (Type I collagen) [37] in response to DEE exposure [38]. The altered expression of these proteins is in fact an indication of a structural damage of the skin tissue. Clearly, DEE exposure caused a depletion in all three markers expression levels, as confirmed by the quantification of the fluorescence staining intensity. However, pre-treatment with SP $PP_{0.5}$ could prevent the loss in filaggrin expression levels compared to DEE samples (Fig. 3A), suggesting that this formulation is able to counteract the cutaneous barrier damage induced by the environmental pollutant exposure. On the other hand, SP $CR_{0.5}$ was unable to prevent stress-induced filaggrin loss promoted by DEE exposure. An opposite trend could be observed in the case of involucrin (Fig. 3B), in which topical application of SP $CR_{0.5}$ significantly prevent the decrease in involucrin expression levels in comparison with untreated biopsies exposed to the

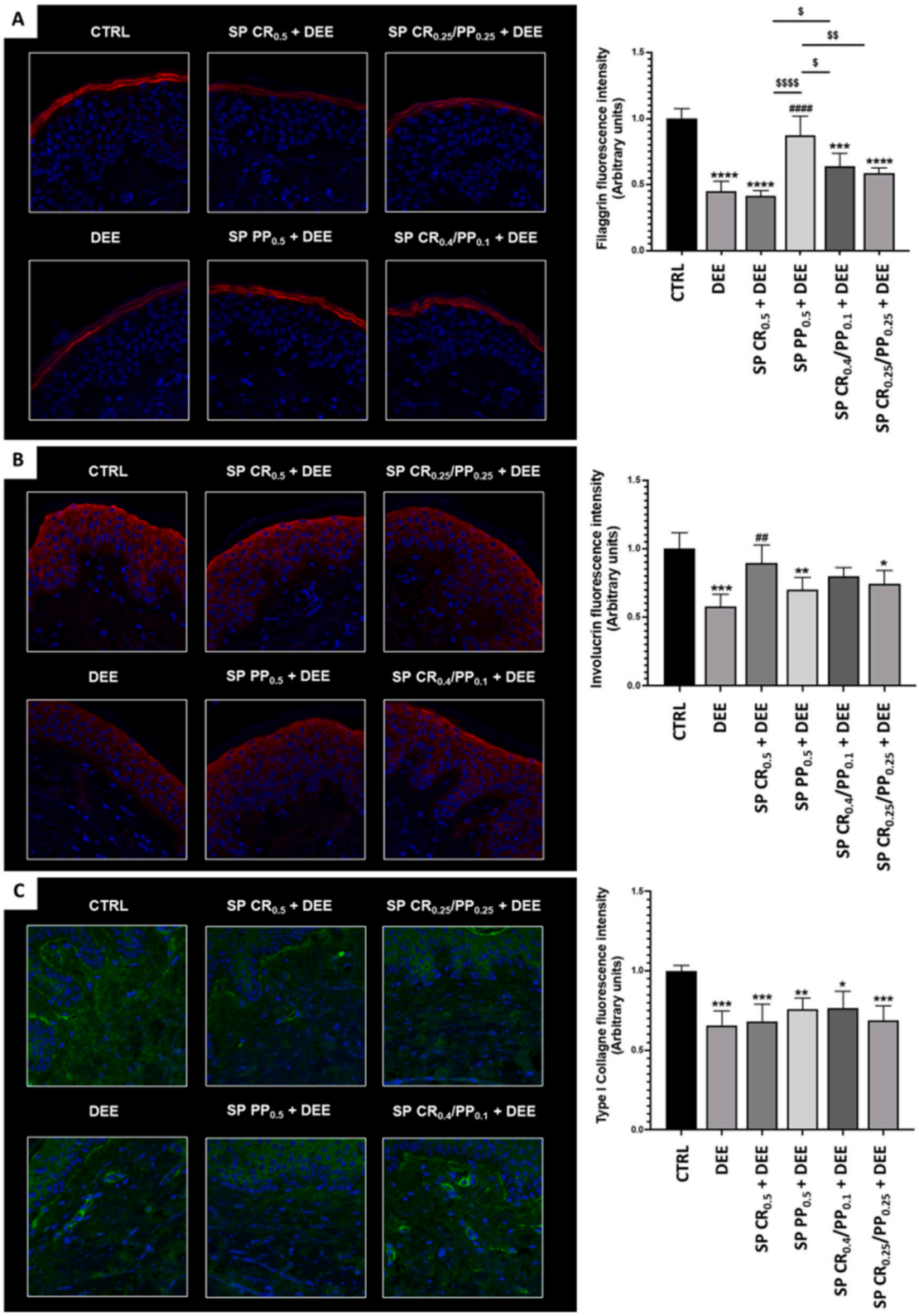

Fig. 3. Immunofluorescence staining for filaggrin (A), involucrin (B), and type I collagen (C) in human skin biopsies treated with the indicated formulations and exposed or not to DEE. Red or green staining represents the indicated proteins, and the blue staining (DAPI) represents nuclei. Images were taken at 40× magnification. The fluorescent signal of the different markers was quantified using ImageJ software 1.53a (Java 1.8.0_172) and expressed in the graphs. Data are the results of the averages of at least three different experiments, with:*,$, $p < 0.05$;**, $$,##, $p < 0.005$; ***, $p = 0.0001$; and ****,####,$$$$, $p < 0.0001$, by 2-way ANOVA followed by Tukey's post hoc comparison test [35]. DEE, SP $CR_{0.5}$, SP $PP_{0.5}$, SP $CR_{0.25}/PP_{0.25}$, SP $CR_{0.4}/PP_{0.1}$, vs. CTRL (*); CTRL, SP $CR_{0.5}$, SP $PP_{0.5}$, SP $CR_{0.25}/PP_{0.25}$, SP $CR_{0.4}/PP_{0.1}$ vs. DEE (#); SP $CR_{0.5}$, SP $CR_{0.25}/PP_{0.25}$, SP $CR_{0.4}/PP_{0.1}$ vs. SP $PP_{0.5}$ and SP $CR_{0.5}$ vs SP $CR_{0.4}/PP_{0.1}$ ($). (For interpretation of the references to colour in this figure legend, the reader is referred to the web version of this article.)

pollutant (DEE); whilst SP $PP_{0.5}$ showed almost no protective effect against involucrin loss. Noteworthily, SP $CR_{0.4}/PP_{0.1}$, showed a more pronounced protective effect against DEE with respect to SP $CR_{0.25}/PP_{0.25}$, suggesting a higher efficacy due to the higher CR amount. Regarding Type I collagen expression, on the contrary, no significant difference between treated and untreated tissues was detected by 2-way ANOVA analysis (Fig. 3C). However, it is still possible to recognize a trend from the graph, which suggest a slightly protective effect exerted especially by SP $CR_{0.4}/PP_{0.1}$.

As previously demonstrated [25], DEE exposure decreases both filaggrin and involucrin levels. This study highlighted that pre-treatment with SP $PP_{0.5}$ efficaciously prevented filaggrin loss, while pre-treatment with SP $CR_{0.5}$ could better prevent involucrin depletion promoted by DEE exposure. In both cases, SP $CR_{0.4}/PP_{0.1}$ showed a higher protective effect with respect to SP $CR_{0.25}/PP_{0.25}$, indicating the 1:4 *w*/w CR-PIP association seems more efficient with respect to the 1:1 w/w association. Interestingly, in the case of the filaggrin marker, CR alone had no effect, while the association with the smaller amount of PP and higher CR was even found to be the most effective, suggesting that PP might promote an enhanced diffusion of CR through the skin, thus favouring its protective effect against DEE already after a short exposure time (48 h), as recently found in the case of ethosomes [14]. Like filaggrin and involucrin, DEE exposure caused a strong depletion in type I collagen expression, confirming the harmful action of the pollutant, even after a short exposure. The slight increase in type I collagen levels compared to DEE exposed in the case of SP $PP_{0.5}$ and SP $CR_{0.4}/PP_{0.1}$ suggests a protective action of the formulations after prolonged treatment. However, considering that the process of skin aging is due to a continuous and prolonged exposure to environmental pollutants, 48 h of exposure to DEE may not yet be sufficient to appreciate a significant protective effect of the formulations. Moreover, it is likely that, over the duration of the experiment, CR and PP were not able to penetrate deep enough to carry out their protective action on the dermis. In contrast, the action of the formulation was more effective on the superficial layers of the epidermis, as evidenced by the levels of the markers filaggrin and involucrin. In this regard, a further ex-vivo long-term study will be required.

4. Conclusions

SP represent versatile and efficient delivery systems for natural antioxidants such as CR and PP. SP ability to protect the skin from pollution-induced damage suggests their potential in advanced skincare products. The data indeed suggest an enhanced diffusion of CR promoted by SP. Considering the short-term study conducted here, a possible long-term efficacy of the spongosome formulation could then be proposed to confirm the protective effects of CR- and PP-loaded SP against various environmental stressors, including UV radiation, ozone, and cigarette smoke in the daily life. These findings may offer new opportunities for future research, mechanistic investigations, formulation optimization, and clinical trials, to validate the clinical efficacy and safety of these innovative dermatological formulations.

Institutional Review Board Statement

The study was conducted according to the guidelines of the Declaration of Helsinki and approved by the Ethics Committee of the University of Ferrara, Italy (protocol code: 170583; date of approval: 16 November 2017).

Informed consent statement

Informed consent was obtained from all subjects involved in the study.

Author statement

All the authors approved the revised version of the manuscript.

CRediT authorship contribution statement

Agnese Bondi: Writing – original draft, Methodology, Investigation, Data curation. **Francesca Ferrara:** Writing – review & editing, Writing – original draft, Methodology, Investigation. **Walter Pula:** Methodology, Data curation. **Paolo Mariani:** Investigation. **Alessia Pepe:** Investigation. **Markus Drechsler:** Investigation. **Leda Montesi:** Methodology, Formal analysis. **Stefano Manfredini:** Writing – review & editing, Resources. **Giuseppe Valacchi:** Writing – review & editing, Validation, Supervision, Project administration, Data curation, Conceptualization. **Elisabetta Esposito:** Writing – review & editing, Project administration, Data curation, Conceptualization.

Declaration of competing interest

The authors declare that they have no known competing financial interests or personal relationships that could have appeared to influence the work reported in this paper.

Data availability

Data will be made available on request.

Acknowledgements

This research was funded by PRIN 2022MC2SKF Italian Ministry of University and Research, European Union, Next Generation EU. The authors thank the Italian National Operational Programme (PON) “Research and Innovation” 2014–2020 financed under ESF resources – REACT EU. The authors acknowledge the CERIC-ERIC Consortium for the access to ELETTRA experimental facility and financial support. PM and AP thank the European Union - Next Generation EU for partial funding (Project code: ECS00000041/I33C22001330007, Project title: Innovation, digitalization and sustainability for the diffused economy in Central Italy - VITALITY).

Appendix A. Supplementary data

Supplementary data to this article can be found online at https://doi.org/10.1016/j.colcom.2024.100811.

References

[1] G. Valacchi, C. Sticozzi, A. Pecorelli, F. Cervellati, C. Cervellati, E. Maioli, Cutaneous responses to environmental stressors, Ann. N. Y. Acad. Sci. 1271 (2012) 75–81, https://doi.org/10.1111/J.1749-6632.2012.06724.X.
[2] X. Gu, Z. Li, J. Su, Air pollution and skin diseases: a comprehensive evaluation of the associated mechanism, Ecotoxicol. Environ. Saf. 278 (2024), https://doi.org/10.1016/J.ECOENV.2024.116429.
[3] F. Ferrara, B. Woodby, A. Pecorelli, M.L. Schiavone, E. Pambianchi, N. Messano, J. P. Therrien, H. Choudhary, G. Valacchi, Additive effect of combined pollutants to UV induced skin OxInflammation damage. Evaluating the protective topical application of a cosmeceutical mixture formulation, Redox Biol. 34 (2020), https://doi.org/10.1016/J.REDOX.2020.101481.
[4] C.A. Weitekamp, L.B. Kerr, L. Dishaw, J. Nichols, M. Lein, M.J. Stewart, A systematic review of the health effects associated with the inhalation of particle-filtered and whole diesel exhaust, Inhal. Toxicol. 32 (2020) 1–13, https://doi.org/10.1080/08958378.2020.1725187.
[5] F. Papaccio, A. D'arino, S. Caputo, B. Bellei, Focus on the contribution of oxidative stress in skin aging, Antioxidants (Basel) 11 (2022), https://doi.org/10.3390/ANTIOX11061121.
[6] J.M. Jaffri, Reactive oxygen species and antioxidant system in selected skin disorders, Malays, J. Med. Sci. 30 (2023) 7–20, https://doi.org/10.21315/MJMS2023.30.1.2.
[7] S.J. Hewlings, D.S. Kalman, Curcumin: a review of its effects on human health, Foods 6 (2017), https://doi.org/10.3390/FOODS6100092.

[8] T. Akanchise, A. Angelova, Potential of Nano-Antioxidants and Nanomedicine for Recovery from Neurological Disorders Linked to Long COVID Syndrome, Antioxidants 12 (2023) 393, https://doi.org/10.3390/ANTIOX12020393.
[9] L. Vollono, M. Falconi, R. Gaziano, F. Iacovelli, E. Dika, C. Terracciano, L. Bianchi, E. Campione, Potential of curcumin in skin disorders, Nutrients 11 (2019), https://doi.org/10.3390/NU11092169.
[10] S. Prasad, A.K. Tyagi, B.B. Aggarwal, Recent developments in delivery, bioavailability, absorption and metabolism of curcumin: the golden pigment from golden spice, Cancer Res. Treat. 46 (2014) 2–18, https://doi.org/10.4143/CRT.2014.46.1.2.
[11] I.U. Haq, M. Imran, M. Nadeem, T. Tufail, T.A. Gondal, M.S. Mubarak, Piperine: a review of its biological effects, Phytother. Res. 35 (2021) 680–700, https://doi.org/10.1002/PTR.6855.
[12] P. Gohil, A. Mehta, Molecular targets of pepper as bioavailability enhancer, Adv. Tradit. Med. 9 (2009) 269–276, https://doi.org/10.3742/OPEM.2009.9.4.269.
[13] C. Jantarat, P. Sirathanarun, S. Boonmee, W. Meechoosin, H. Wangpittaya, Effect of Piperine on Skin Permeation of Curcumin from a Bacterially Derived Cellulose-Composite Double-Layer Membrane for Transdermal Curcumin Delivery, Sci. Pharm. 86 (2018) 39, https://doi.org/10.3390/SCIPHARM86030039.
[14] F. Ferrara, A. Bondi, W. Pula, C. Contado, A. Baldisserotto, S. Manfredini, P. Boldrini, M. Sguizzato, L. Montesi, M. Benedusi, G. Valacchi, E. Esposito, Ethosomes for curcumin and Piperine cutaneous delivery to prevent environmental-stressor-induced skin damage, Antioxidants 13 (2024) 91, https://doi.org/10.3390/ANTIOX13010091/S1.
[15] C.V. Kulkarni, W. Wachter, G. Iglesias-Salto, S. Engelskirchen, S. Ahualli, Monoolein: a magic lipid? Phys. Chem. Chem. Phys. 13 (2011) 3004–3021, https://doi.org/10.1039/C0CP01539C.
[16] G. Blanco-Fernández, B. Blanco-Fernandez, A. Fernández-Ferreiro, F.J. Otero-Espinar, Lipidic lyotropic liquid crystals: insights on biomedical applications, Adv. Colloid Interf. Sci. 313 (2023) 102867, https://doi.org/10.1016/J.CIS.2023.102867.
[17] N. Akombaetwa, A.B. Ilangala, L. Thom, P.B. Memvanga, B.A. Witika, A.B. Buya, Current advances in lipid Nanosystems intended for topical and transdermal drug delivery applications, Pharmaceutics 15 (2023), https://doi.org/10.3390/PHARMACEUTICS15020656.
[18] L.B. Lopes, M.T.J. Garcia, M.V. Lb Bentley, Chemical penetration enhancers, Ther. Deliv. 6 (2015) 1053–1061, https://doi.org/10.4155/TDE.15.61.
[19] M. Rakotoarisoa, B. Angelov, M. Drechsler, V. Nicolas, T. Bizien, Y.E. Gorshkova, Y. Deng, A. Angelova, Liquid crystalline lipid nanoparticles for combined delivery of curcumin, fish oil and BDNF: in vitro neuroprotective potential in a cellular model of tunicamycin-induced endoplasmic reticulum stress, Smart Mater Med 3 (2022) 274–288, https://doi.org/10.1016/J.SMAIM.2022.03.001.
[20] M. Rakotoarisoa, B. Angelov, V.M. Garamus, A. Angelova, Curcumin- and fish oil-loaded Spongosome and Cubosome nanoparticles with neuroprotective potential against H 2 O 2 -induced oxidative stress in differentiated human SH-SY5Y cells, ACS Omega 4 (2019) 3061–3073, https://doi.org/10.1021/ACSOMEGA.8B03101/ASSET/IMAGES/MEDIUM/AO-2018-031015_M002.GIF.
[21] G. Valacchi, F. Virgili, C. Cervellati, A. Pecorelli, OxInflammation: from subclinical condition to pathological biomarker, Front. Physiol. 9 (2018), https://doi.org/10.3389/FPHYS.2018.00858.
[22] E. Esposito, L. Calderan, A. Galvan, E. Cappellozza, M. Drechsler, P. Mariani, A. Pepe, M. Sguizzato, E. Vigato, E. Dalla Pozza, M. Malatesta, Ex Vivo Evaluation of Ethosomes and Transethosomes Applied on Human Skin: A Comparative Study, Int. J. Mol. Sci. 23 (2022) 15112, https://doi.org/10.3390/IJMS232315112.
[23] M. Sicurella, W. Pula, K. Musiał, K. Cieślik-Boczula, M. Sguizzato, A. Bondi, M. Drechsler, L. Montesi, E. Esposito, P. Marconi, Ethosomal gel for topical Administration of Dimethyl Fumarate in the treatment of HSV-1 infections, Int. J. Mol. Sci. 24 (2023) 4133, https://doi.org/10.3390/IJMS24044133/S1.
[24] J. Ivarsson, F. Ferrara, A. Vallese, A. Guiotto, S. Colella, A. Pecorelli, G. Valacchi, Comparison of pollutant effects on cutaneous Inflammasomes activation, Int. J. Mol. Sci. 24 (2023) 16674, https://doi.org/10.3390/IJMS242316674/S1.
[25] E. Pambianchi, F. Ferrara, A. Pecorelli, M. Benedusi, H. Choudhary, J.P. Therrien, G. Valacchi, Deferoxamine Treatment Improves Antioxidant Cosmeceutical Formulation Protection against Cutaneous Diesel Engine Exhaust Exposure, Antioxidants 10 (2021) 1928, https://doi.org/10.3390/ANTIOX10121928.
[26] Z. Wu, X. Tang, S. Liu, S. Li, X. Zhao, Y. Wang, X. Wang, H. Li, Mechanism underlying joint loading and controlled release of β-carotene and curcumin by octenylsuccinated Gastrodia elata starch aggregates, Food Res. Int. 172 (2023) 113136, https://doi.org/10.1016/J.FOODRES.2023.113136.
[27] E. Esposito, C. Sticozzi, L. Ravani, M. Drechsler, X.M. Muresan, F. Cervellati, R. Cortesi, G. Valacchi, Effect of new curcumin-containing nanostructured lipid dispersions on human keratinocytes proliferative responses, Exp. Dermatol. 24 (2015), https://doi.org/10.1111/exd.12696.
[28] B. Angelov, A. Angelova, R. Mutafchieva, S. Lesieur, U. Vainio, V.M. Garamus, G. V. Jensen, J.S. Pedersen, SAXS investigation of a cubic to a sponge (L3) phase transition in self-assembled lipid nanocarriers, Phys. Chem. Chem. Phys. 13 (2011) 3073–3081, https://doi.org/10.1039/C0CP01029D.
[29] P. Mariani, V. Luzzati, H. Delacroix, Cubic phases of lipid-containing systems. Structure analysis and biological implications, J. Mol. Biol. 204 (1988) 165–189, https://doi.org/10.1016/0022-2836(88)90607-9.
[30] J. Gustafsson, T. Nylander, M. Almgren, Phase behavior and aggregate structure in aqueous mixtures of sodium cholate and glycerol Monooleate, J. Colloid Interface Sci. 211 (1999) 326–335, https://doi.org/10.1006/JCIS.1998.5996.
[31] M. Rakotoarisoa, B. Angelov, S. Espinoza, K. Khakurel, T. Bizien, M. Drechsler, A. Angelova, Composition-switchable liquid crystalline nanostructures as green formulations of curcumin and fish oil, ACS Sustain. Chem. Eng. 9 (2021) 14821–14835, https://doi.org/10.1021/ACSSUSCHEMENG.1C04706/ASSET/IMAGES/MEDIUM/SC1C04706_0009.GIF.
[32] V. Luzzati, R. Vargas, P. Mariani, A. Gulik, H. Delacroix, Cubic phases of lipid-containing systems. Elements of a theory and biological connotations, J. Mol. Biol. 229 (1993) 540–551, https://doi.org/10.1006/JMBI.1993.1053.
[33] S. Mazzoni, L.R.S. Barbosa, S.S. Funari, R. Itri, P. Mariani, Cytochrome-c affects the Monoolein polymorphism: consequences for stability and loading efficiency of drug delivery systems, Langmuir 32 (2016) 873–881, https://doi.org/10.1021/ACS.LANGMUIR.5B03507.
[34] E. Esposito, L. Ravani, P. Mariani, C. Contado, M. Drechsler, C. Puglia, R. Cortesi, Curcumin containing monoolein aqueous dispersions: a preformulative study, Mater. Sci. Eng. C 33 (2013) 4923–4934, https://doi.org/10.1016/J.MSEC.2013.08.017.
[35] G.F. Murphy, T.C. Flynn, R.H. Rice, G.S. Pinkus, Involucrin expression in normal and neoplastic human skin: a marker for keratinocyte differentiation, J. Invest. Dermatol. 82 (1984) 453–457, https://doi.org/10.1111/1523-1747.EP12260945.
[36] A. Sandilands, C. Sutherland, A.D. Irvine, W.H.I. McLean, Filaggrin in the frontline: role in skin barrier function and disease, J. Cell Sci. 122 (2009) 1285–1294, https://doi.org/10.1242/JCS.033969.
[37] L. Gardeazabal, A. Izeta, Elastin and collagen fibres in cutaneous wound healing, Exp. Dermatol. 33 (2024) e15052, https://doi.org/10.1111/EXD.15052.
[38] D. McDaniel, P. Farris, G. Valacchi, Atmospheric skin aging-contributors and inhibitors, J. Cosmet. Dermatol. 17 (2018) 124–137, https://doi.org/10.1111/JOCD.12518.